CONFERENCE PRE-PRINT

IMPURITY RADIATION SEEDING OF NEOCLASSICAL TEARING MODE GROWTH

S.Y. ZENG

International Joint Research Laboratory of Magnetic Confinement Fusion and Plasma Physics, State Key Laboratory of Advanced Electromagnetic Technology, Huazhong University of Science and Technology Wuhan, Hubei, China

P. ZHU

International Joint Research Laboratory of Magnetic Confinement Fusion and Plasma Physics, State Key Laboratory of Advanced Electromagnetic Technology, Huazhong University of Science and Technology Wuhan, Hubei, China University of Wisconsin-Madison Madison, Wisconsin, United States of America Email: zhup@hust.edu.cn

E. C. HOWELL

Tech-X Corporation

Boulder, Colorado, United States of America

Abstract

The physics of neoclassical tearing modes (NTMs) is a major concern for tokamak plasma stability and performance, particularly in the burning plasma regime. While seed events such as sawteeth and edge localized modes can often be clearly identified, the potential seeding of NTMs through resistive tearing instability driven by impurity radiation cooling still requires further investigation. Recent NIMROD simulations have shown that local impurity radiation cooling can drive seed island growth and trigger subsequent NTM instability. This seed island is primarily driven by the local helical perturbation of the diamagnetic current, which results from the perturbed pressure gradient due to impurity radiative cooling near the rational surface. A heuristic closure for the neoclassical viscosity is adopted, and the seed island is further driven by the perturbed bootstrap current arising from the neoclassical electron viscous stress within the extended Ohm's law. The growth rate of the NTM in simulations is found to be proportional to the electron neoclassical viscosity, and a theoretical neoclassical driving term is used to account for the nonlinear neoclassical island growth observed in the simulations. The detrimental effects arising from the persistent NTM growth in the burning plasma regime are evaluated.

1. INTRODUCTION

Since the first observation of the neoclassical tearing mode (NTM) on TFTR [1], it is well established that NTMs are detrimental to fusion plasmas [2][3][4][5]. Empirical scaling indicates that the marginal beta limit for NTM growth is nearly linearly proportional to the normalized ion gyro-radius $\rho_i^* = (M_i v_i/q_i B)/a$ (where M_i , v_i , and q_i are the ion mass, velocity, and charge, respectively; B is the magnetic field; and a is the minor radius). This scaling predicts a very low beta threshold in future large tokamak devices [6][7]. For example, based on the JET scaling law $\beta_N = 95.5 \rho_i^{*0.71\pm0.14}$ for sawtooth-triggered 3/2 NTM onset, the marginal beta in ITER plasma is predicted to be $\beta_N \sim 0.7$ with $\rho_i^* \sim 1 \times 10^{-3}$ [7][8]. Additionally, the required seed island width for NTM onset in ITER plasma is predicted to be 1-2 cm [5].

The mechanism behind seed island creation for NTM onset and growth remains an active area of research, particularly in developing theory-based predictive capabilities and explaining why certain seed events trigger NTMs while others do not. Previous studies have proposed that seed islands are triggered by precursor MHD instabilities such as sawteeth [9][10][11], fishbones [9], edge-localized modes [5], and infernal modes [12]. Spontaneous NTM onset in the absence of detectable precursor MHD events has also been reported [13][14][15][16], where the tearing index Δ' becomes extremely large and positive as the equilibrium approaches the ideal stability boundary. TCV experiments have demonstrated that NTMs can grow from current-driven tearing modes [17]. Other suggested seeding mechanisms include mode coupling [18][19], resonant magnetic perturbations [20][21][22], and turbulence [23][24][25]. Two main theoretical models—the finite thermal transport model and the polarization current model—have been developed to explain NTM onset [26][27]. Comparisons between theory and experiment are challenging due to difficulties in detecting thin seed islands and accurately measuring driving terms in NTM models that depend on local quantities at the rational surface.

Impurity radiation plays a crucial role in steady-state tokamak operation and has been confirmed in numerous experiments to drive tearing mode instability [28][29][30][31]. A nonlinear theory based on cylindrical geometry has been developed to interpret this thermo-resistive tearing instability [32][33][34], and the impurity radiation-driven tearing mode growth has been numerically studied using codes such as NIMROD [34][35][36], JOREK [37][38], M3D-C¹[39], and others [40][41][42]. Naturally, the impurity radiation-induced resistive tearing mode could be a potential seed mechanism for NTMs. For instance, JET experiments have shown tearing mode onset due to current density profile modifications following changes in the electron temperature profile from radiative cooling [43]. However, experimental observations so far only indicate a correlation between impurity radiation and potential NTM growth, with the detailed underlying physics remaining unclear. This work aims to explore a radiation-driven seeding mechanism for NTM onset by demonstrating local impurity radiation cooling-induced seed island growth and subsequent bootstrap current-driven neoclassical tearing growth, particularly in the burning plasma regime where the effects from the α -particle heating and Helium ash radiation cooling are inevitable yet unknown.

2. SIMULATION MODEL

Our simulations are based on the single-fluid resistive MHD model implemented in the NIMROD code [44], which incorporates an atomic physics module ported from the KPRAD code to calculate the particle and energy sources due to the impurity ionization, recombination and radiation processes [45][46], and a heuristic closure for the neoclassical viscosities [47][48]:

$$\rho \frac{d\vec{V}}{dt} = -\nabla p + \vec{J} \times \vec{B} + \nabla \cdot (\rho \nu \nabla \vec{V}) - \nabla \cdot \vec{\Pi}_i, \tag{1}$$

$$\frac{dn_i}{dt} + n_i \nabla \cdot \vec{V} = \nabla \cdot (D \nabla n_i) + S_{ion/rec}, \tag{2}$$

$$\frac{dn_z}{dt} + n_z \nabla \cdot \vec{V} = \nabla \cdot (D \nabla n_z) + S_{ion/rec}, \tag{3}$$

$$n_e \frac{dT_e}{dt} = (\gamma - 1) \left[n_e T_e \nabla \cdot \vec{V} + \nabla \cdot \vec{q}_e - Q \right], \tag{4}$$

$$\vec{q}_e = -n_e \left[\kappa_{\parallel} \vec{b} \vec{b} + \kappa_{\perp} (\mathcal{I} - \vec{b} \vec{b}) \right] \cdot \nabla T_e, \tag{5}$$

$$\frac{\partial \vec{B}}{\partial t} = -\nabla \times \vec{E}, \qquad \nabla \times \vec{B} = \mu_0 \vec{J}, \tag{6}$$

$$\vec{E} = -\vec{V} \times \vec{B} + \eta \vec{J} - \frac{1}{en_e} \nabla \cdot \vec{\Pi}_e. \tag{7}$$

Here, n_i , n_e , and n_z are the main ion, electron, and impurity ion number densities respectively, e, ρ , \vec{V} , \vec{J} , and p the electron charge, the plasma mass density, velocity, current density, and pressure respectively, T_e and \vec{q}_e the electron temperature and heat flux respectively, D, v, η , and κ_{\parallel} (κ_{\perp}) the plasma diffusivity, kinematic viscosity, resistivity, and parallel (perpendicular) thermal conductivity respectively, $\gamma = 5/3$ the adiabatic index, $S_{ion/rec}$ the density source, Q the energy source, \vec{E} (\vec{B}) the electric (magnetic) field, $\vec{b} = \vec{B}/B$, \mathcal{I} the unit dyadic tensor, and $\vec{\Pi}_e$ ($\vec{\Pi}_i$) the electron (ion) neoclassical viscous stress tensor. The heuristic closure is able to capture the main characteristics of NTM growth [47][48], and thus may serve as a proxy to the more complete kinetic-MHD models that are still under development [50]. The simulations are based on the hybrid scenario design of China Fusion Engineering Test Reactor (CFETR) [51].

IMPURITY RADIATION INDUCED SEED ISLAND

First, we examine simulations with varying levels of local impurity density without the neoclassical closure (Fig. 1). A neutral neon gas source is deposited at the q=2 rational surface at the beginning of the simulation (t=0 ms). The initial impurity source follows a Gaussian distribution along the toroidal direction, exciting a strong n=1mode perturbation, and the impurity distribution remains asymmetric throughout the simulation. Both the

width and growth rate of the impurity radiation-induced magnetic island are proportional to the impurity density level (Fig. 1a) and the corresponding local impurity radiation power (Fig. 1b). At low impurity density, the island saturates at a very small size. Due to anisotropic thermal conductivity, the island separatrix shields the heat flux from the external background plasma, confining the thermal energy inside the island, which is governed by the local balance between radiative cooling and Ohmic heating.

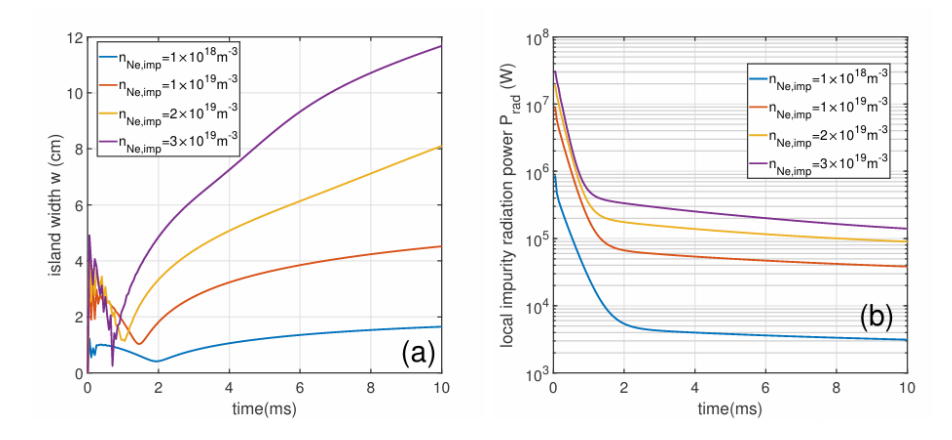


FIG. 1. (a) The island width of the 2/1 mode and (b) the local impurity radiation power on the q=2 surface as functions of time with various impurity density levels.

We now analyze in detail the case of small island growth $(n_{Ne,imp}=1\times 10^{19}m^{-3})$ to elucidate the effects of local impurity radiation cooling. A large radiation power peak occurs initially, dominated by line radiation from the neutral source, which decays rapidly as ionization increases (yellow region in Fig. 2a). This peak induces strong perturbations to the plasma equilibrium on the thermal transport timescale, much shorter than the resistive diffusion time. The seeding process occurs between t=0 ms and t=1 ms, with no pre-existing island at t=0. The strong impurity radiation cooling dominates this early phase (t \leq 1.5ms), leading to the formation of a seed island. After t>1.5 ms, the tearing mode becomes the dominant instability. The island growth rate dw/dt increases rapidly to a maximum before gradually approaching a steady value (Fig. 2b). The tearing stability parameter Δ' at the resonant surface evolves similarly, rising sharply to a positive maximum from negative values and then decaying slowly. This parameter is measured as

$$\Delta' = \left[\frac{dB_r^{2/1}}{dr} \bigg|_{r_s^+} - \frac{dB_r^{2/1}}{dr} \bigg|_{r_s^-} \right] / B_r^{2/1}(r_s). \tag{8}$$

Where r_s , r_s^+ , r_s^- denote the radial location of the rational surface and its immediate right and left sides, respectively. $B_r^{2/1}$ is the m=2/n=1 radial component of the perturbed magnetic field. The evolution of Δ' is consistent with the Rutherford model $\tau_R dw/dt \sim \Delta'$ for most of the time, except near the peak growth where non-inductive contributions become significant. In this region, Δ' should be replaced with $\Delta' - \Delta'_c$, accounting for the Glasser resistive interchange correction due to toroidal curvature effects [52]. This stabilizing effect is significant during early island growth when linear Δ' peaks, explaining the gap between Δ' and the actual growth rate (Fig. 2b). Essentially, Δ' represents a simplification of Ampère's law: $\Delta'\psi\simeq\int\nabla^2\psi dr\simeq\int\delta Jdr$, where ψ is the perturbed magnetic flux and δJ is the helical current density perturbation within the tearing layer. Using an extended definition, Δ'_r is calculated at mid-radius in discrete layers around the rational surface to approximate the current density perturbation in each layer (Fig. 2c). The measured Δ' includes contributions from current perturbations induced by local impurity radiation cooling, primarily through modifications of the local pressure profile around the rational surface. Based on the modified force balance $dp_1/dr = J_1 \times B_0 + J_0 \times B_1$, where the second term is negligible, the perpendicular current perturbation $J_{1\perp} \simeq \frac{1}{B_0} dp_1/dr$ contributes to the parallel current perturbation $J_{1\parallel}$ via quasi-neutrality condition $\nabla \cdot \overrightarrow{J_1} = 0$.

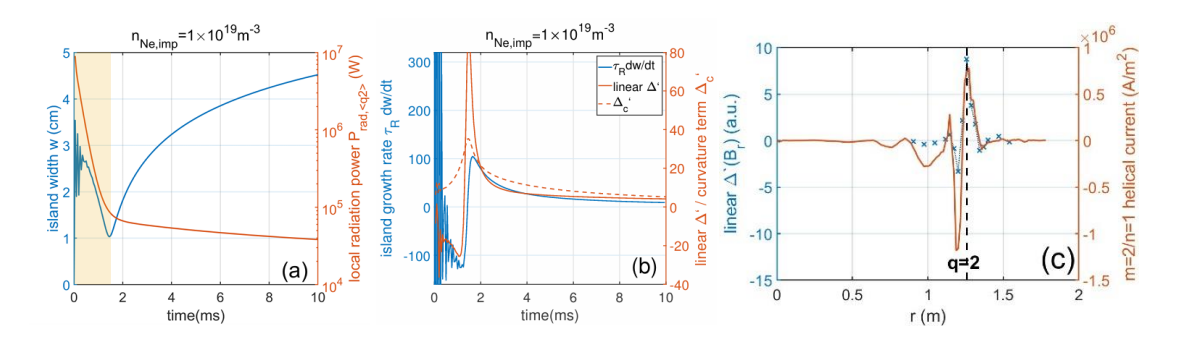


FIG. 2. (a) The island width of the 2/1 mode and the local impurity radiation power on the q=2 surface, and (b) the island growth rate of the 2/1 mode, the linear tearing stability parameter Δ' and the curvature term Δ'_c as functions of time. (c) The radial profile of the 2/1 component of helical current density, and the discrete values of the linear Δ'_r calculated in each of the discrete layer around the rational surface using Eq. (8), the blue dotted line shows the variation of the Δ'_r . The q=2 surface is indicated by the vertical black dashed line, and t=2.5 ms.

4. IMPURITY RADIATION SEEDED NONLINEAR TEARING MODE GROWTH

In presence of the heuristic neoclassical closure, the growth of the impurity radiation-seeded island is further driven by the perturbed bootstrap current, which originates from the neoclassical electron stress in the extended Ohm's law. As shown in Fig. 3(a), a threshold is identified in the coefficient μ_e ($\mu_e = 1 \times 10^6 s^{-1}$), above which the seed island begins to grow rather than continue to decay. Higher values of μ_e lead to larger growth rates. The inclusion of the heuristic neoclassical closure is directly responsible for this nonlinear island growth (Fig. 3b).

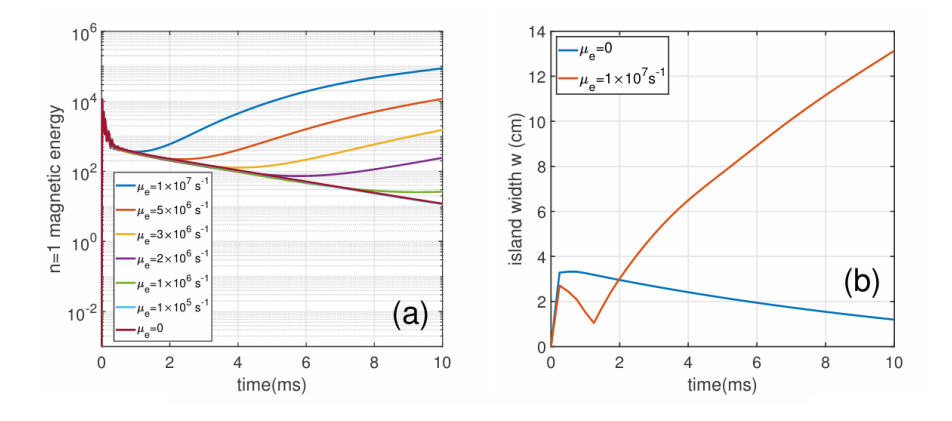


FIG. 3. (a) The magnetic energy of the n=1 component of perturbation and (b) the island width of the 2/1 mode with various values of the coefficient μ_e as functions of time.

A simplified theoretical model for the perturbed bootstrap current, $\delta J_{bs} = \epsilon^{1/2}/B_{\theta}(d\delta p/dr)$ (where ϵ is the inverse aspect ratio), is generally consistent with the total current perturbations from simulations in the NTM growth case (Fig. 4a). In comparison, the current perturbation in the resistive tearing mode case is much smaller. The additional current perturbation in the neoclassical case is attributed to the heuristic electron force $\nabla \cdot \vec{\Pi}_e/(en_e)$ driving the bootstrap current perturbation in the extended Ohm's law. Differences between the theoretical model and simulation results arise because the simulations include not only the dominant bootstrap current perturbation but also other contributions, such as the perturbed Pfirsch–Schlüter current δJ_{ps} . However, the latter's contribution is small since $\delta J_{ps}/\delta J_{bs} \sim \epsilon^{1/2}$ [53], based on the assumption $\epsilon \ll 1$. It is important to note that impurity density levels—and thus impurity radiation power levels—are maintained equally in both resistive and neoclassical tearing mode cases. Consequently, the impurity radiation cooling-induced pressure gradient perturbations and perturbed Pfirsch–Schlüter currents are comparable in both scenarios. In the modified Rutherford equation, the neoclassical driving term often assumes a simplified form in the large-aspect-ratio limit:

$$\Delta_{bs}' = \frac{\sqrt{\epsilon}}{w} \beta_p \frac{L_q}{L_p},\tag{9}$$

where β_p is the ratio of plasma thermal pressure to poloidal magnetic pressure, $L_q = q/q'$, and $L_p = p/p'$; all values are evaluated at the rational surface [3]. The neoclassical driving term Δ'_{bs} measured from simulation results agrees well with nonlinear island growth in the same simulation (Fig. 4b). Additionally, the tearing stability parameter Δ' remains negative over time in the resistive tearing mode case without neoclassical closure, confirming the metastability of the seed island. In the neoclassical island growth case (with $\mu_e = 1 \times 10^{-7}$), Δ' evaluated via Eq. (8) is not always negative, unlike in the resistive case, as the NTM modifies the current profile, leading to positive Δ' values.

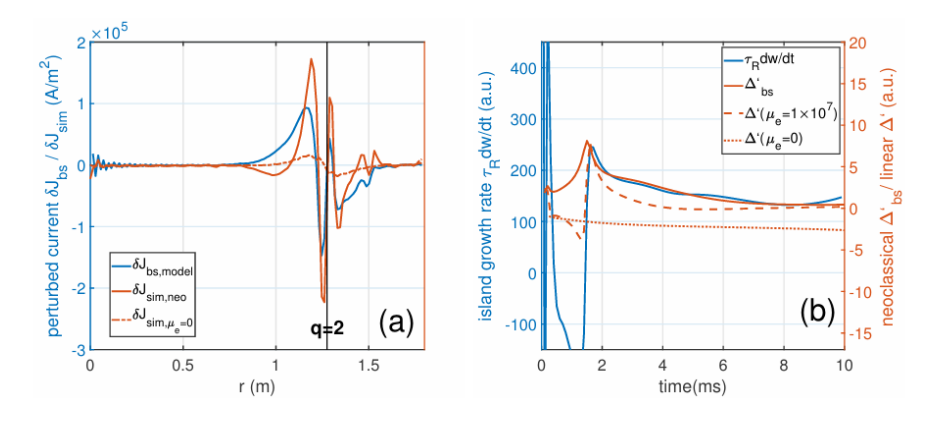


FIG. 4. (a) The radial profiles of the perturbed bootstrap current model $\delta J_{bs} = \epsilon^{1/2}/B_{\theta}(d\delta p/dr)$, the perturbed helical current density from the simulation results with $(\delta J_{sim,neo})$ and without $(\delta J_{sim,\mu_e=0})$ the inclusion of the heuristic neoclassical closure, respectively. (b) The island growth rate of the 2/1 mode, the neoclassical driving term Δ'_{bs} measured from the simulation results, the evaluation of tearing stability parameter Δ' in the neoclassical tearing case ($\mu_e = 1 \times 10^7 \, \text{s}^{-1}$), and the tearing stability parameter Δ' of the resistive tearing case ($\mu_e = 0$) as functions of time.

We employ a highly simplified model to evaluate the scenario of NTM growth in the burning plasma regime. This model incorporates the alpha particle heating power $P_{\alpha}=1/4n_i^2\langle\sigma\nu\rangle_{DT}E_{\alpha}$, where $\langle\sigma\nu\rangle_{DT}$ is the deuterium-tritium fusion reaction rate and $E_{\alpha}=3.15$ MeV is the alpha particle energy, into the energy source term Q in Eq. (4). The model assumes that this energy is completely and instantaneously absorbed locally by the plasma. When considering the radiation from helium ash (rather than localized impurity radiation cooling from pellet injection), the results are shown in Fig. 5. The magnetic island grows gradually toward saturation (Fig. 5a), and the plasma thermal energy drops rapidly once the island width exceeds a certain threshold. The total alpha heating power, which is concentrated in the central plasma region due to peaks in plasma density and temperature, is approximately two orders of magnitude larger than the helium ash radiation power (Fig. 5b)

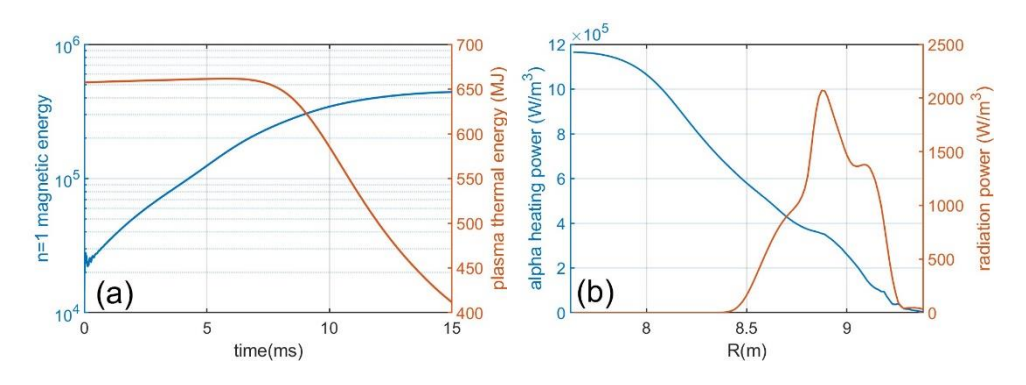


FIG. 5. (a) The magnetic energy of the n = 1 component of perturbation and plasma thermal energy as functions of time. (b) The radial profiles of the alpha heating power and Helium ash radiation power at t = 5 ms.

The growth of the NTM persists even when alpha heating power exceeds radiative cooling, which can be explained by the global profile evolution. The seed island causes local flattening of plasma profiles—such as the electron temperature profile visible at t = 2.5 ms in Fig. 6(a)—which reduces the local bootstrap current drive at the rational surface. However, both the alpha heating and the radiative cooling contribute to global modifications in the plasma kinetic profiles, therefore maintaining locally flattened profiles. This contrasts with the electron

cyclotron current drive, which induces local profile changes that can compensate for the loss of bootstrap current. As the tearing mode instability continues to grow, multiple modes develop in addition to the dominant 2/1 mode (Fig. 6b). This leads to rapid transport of particles and heat from the central plasma region to the edge (Fig. 6a), facilitated by the large magnetic island itself and the stochastic magnetic field resulting from island overlap. It is also important to note that while the present work considers only the temperature perturbations due to alpha heating and radiative cooling, kinetic effects from fast alpha particles—such as their influence on helical current drive—may also significantly affect tearing mode growth.

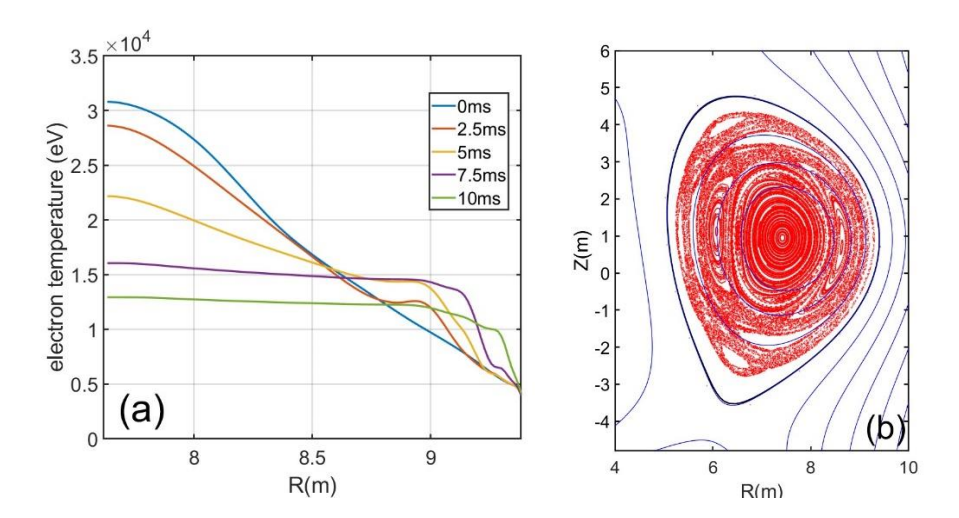


FIG. 6. (a) The radial profiles of the plasma electron temperature at various times and (b) the Poincare plot showing the presence of magnetic island when t=10 ms.

CONCLUSION

In summary, NIMROD simulations demonstrate that local impurity radiation cooling can seed neoclassical tearing modes (NTMs). The physics of this seeding process and the subsequent neoclassical island growth have been demonstrated. The seed island is primarily driven by a local helical current perturbation, which arises mainly from the diamagnetic current induced by the perturbed pressure gradient due to radiative cooling. This perturbation modifies Δ' in the outer region, facilitating nonlinear seed island growth. When a heuristic neoclassical closure is incorporated into the extended Ohm's law, the perturbed bootstrap current—arising from electron neoclassical stress—further drives the island growth in the nonlinear regime. It is demonstrated that in the burning plasma the impurity seeded NTM growth persists even when the α -particle heating dominates the impurity including the Helium ash radiative cooling.

ACKNOWLEDGEMENTS

We are grateful for the supports from the NIMROD team and the CFETR physics design team. This work was supported by the National Magnetic Confinement Fusion Program of China (Grant No. 2019YFE03050004), Hubei International Science and Technology Cooperation Projects (No. 2022EHB003), and U.S. Department of Energy (Grant No. DE-FG02-86ER53218). This research used resources of the National Energy Research Scientific Computing Center, a DOE Office of Science User Facility supported by the Office of Science of the U.S. Department of Energy under Contract No. DE-AC02-05CH11231 using NERSC award FES-ERCAP0027638.

REFERENCES

- [1] Chang Z., Callen J.D., Fredrickson E.D., Budny R.V., Hegna C.C., McGuire K.M. and Zarnstorff M.C. (TFTR Group) 1995 Phys. Rev. Lett. 74 4663–6
- [2] Sauter O. et al 1997 Phys. Plasmas 4 1654-64
- [3] Hegna C.C. 1998 Phys. Plasmas 5 1767-74
- [4] Buttery R.J. et al 2000 Plasma Phys. Control. Fusion 42 B61–B73

- [5] La Haye R.J., Chrystal C., Strait E., Callen J., Hegna C., Howell E., Okabayashi M. and Wilcox R. 2022 Nucl. Fusion 62 056017
- [6] Maraschek M., Sauter O., Günter S. and Zohm H. (ASDEX-Upgrade Team) 2003 Plasma Phys. Control. Fusion 45 1369
- [7] Buttery R., Hender T., Howell D., Haye R.L., Sauter O. and Testa D. (Contributors to the EFDA-JET Work programme) 2003 Nucl. Fusion 43 69
- [8] La Haye R.J., Buttery R.J., Guenter S., Huysmans G.T.A., Maraschek M. and Wilson H.R. 2000 Phys. Plasmas 7 3349– 59
- [9] Gude A., Günter S. and Sesnic S. (ASDEX Upgrade Team) 1999 Nucl. Fusion 39 127
- [10] Sauter O. et al 2002 Phys. Rev. Lett. 88 105001
- [11] Canal G., Duval B., Felici F., Goodman T., Graves J., Pochelon A., Reimerdes H., Sauter O. and Testa D. (the TCV Team) 2013 Nucl. Fusion 53 113026
- [12] Kleiner A., Graves J., Brunetti D., Cooper W., Halpern F., Luciani J.-F. and Lütjens H. 2016 Nucl. Fusion 56 092007
- [13] Fredrickson E.D. 2002 Phys. Plasmas 9 548–59
- [14] Brennan D.P., Strait E.J., Turnbull A.D., Chu M.S., La Haye R.J., Luce T.C., Taylor T.S., Kruger S. and Pletzer A. 2002 Phys. Plasmas 9 2998–3006
- [15] Brennan D.P. et al 2003 Phys. Plasmas 10 1643–52
- [16] Brennan D., Kruger S., Gianakon T. and Schnack D. 2005 Nucl. Fusion 45 1178
- [17] Reimerdes H., Sauter O., Goodman T. and Pochelon A. 2002 Phys. Rev. Lett. 88 105005
- [18] Bardóczi L., Logan N.C. and Strait E.J. 2021 Phys. Rev. Lett. 127 055002
- [19] Nave M., Lazzaro E., Coelho R., Belo P., Borba D., Buttery R., Nowak S. and Serra F. (EFDA-JET Contributors) 2003 Nucl. Fusion 43 179
- [20] Buttery R., Valovi M., Warrick C. and Wilson H. (COMPASS-D Team and ECRH Teams) 2001 Nucl. Fusion 41 985
- [21] Qu H. et al (the EAST Team) 2022 Nucl. Fusion 62 096007
- [22] Yu Q., Günter S., Lackner K. and Maraschek M. 2012 Nucl. Fusion 52 063020
- [23] Muraglia M., Agullo O., Benkadda S., Yagi M., Garbet X. and Sen A. 2011 Phys. Rev. Lett. 107 095003
- [24] Muraglia M., Agullo O., Poyé A., Benkadda S., Dubuit N., Garbet X. and Sen A. 2017 Nucl. Fusion 57 072010
- [25] Muraglia M., Poyé A., Agullo O., Dubuit N. and Garbet X. 2021 Plasma Phys. Control. Fusion 63 084005
- [26] Zabiego M. and Callen J. 1997 Nucl. Fusion 37 361
- [27] La Haye R.J. and Sauter O. 1998 Nucl. Fusion 38 987
- [28] Suttrop W. et al 1997 Nucl. Fusion 37 119-25
- [29] Salzedas F., Schüller F.C. and Oomens A.A.M. (the RTP Team) 2002 Phys. Rev. Lett. 88 075002
- [30] Delgado-Aparicio L. et al 2011 Nucl. Fusion 51 083047
- [31] Xu L. et al 2017 Nucl. Fusion 57 126002
- [32] Gates D.A. and Delgado-Aparicio L. 2012 Phys. Rev. Lett. 108 1-4
- [33] White R.B., Gates D.A. and Brennan D.P. 2015 Phys. Plasmas 22 022514
- [34] Zeng S., Zhu P., Zhou R. and Escande D.F. 2022 Nucl. Fusion 63 016026
- [35] Zeng S., Zhu P., Zhou R. and Xu M. 2023 Nucl. Fusion
- [36] Zeng S., Zhu P. and Ren H. 2023 Plasma Phys. Control. Fusion 65 125001
- [37] Nardon E., Fil A., Hoelzl M. and Huijsmans G. (JET contributors) 2016 Plasma Phys. Control. Fusion 59 014006
- [38] Wieschollek F., Hoelzl M. and Nardon E. (JOREK Team, ASDEX Upgrade Team, EUROfusion MST1 Team) 2022 Phys. Plasmas 29 032509
- [39] Teng Q., Ferraro N., Gates D. and White R. 2018 Nucl. Fusion 58 106024
- [40] Jiang S., Tang W., Wei L., Liu T., Xu H. and Wang Z. 2022 Plasma Sci. Technol. 24 055101
- [41] Jiang S., Wang Z.X., Wei L. and Liu T. 2023 Chin. Phys. B 32 105203
- [42] Xu H.-W., Zhang H.-W., Song Y.-H., Ma Z.-W. and Wang Y.-N. 2020 Plasma Phys. Control. Fusion 62 105009
- [43] Pucella G. et al (JET Contributors) 2021 Nucl. Fusion 61 046020
- [44] Sovinec C.R. et al 2004 J. Comput. Phys. 195 355-86
- [45] Whyte D.G. et al 1997 Proc. 24th European Conf. on Controlled Fusion and Plasma Physics (9 June–14 June 1996, Berchtesgaden) vol 21A (European Physical Society) p 1137
- [46] Izzo V.A. 2013 Phys. Plasmas 20 056107
- [47] Gianakon T.A., Kruger S.E. and Hegna C.C. 2002 Phys. Plasmas 9 536-47
- [48] Howell E.C., King J.R., Kruger S.E., Callen J.D., La Haye R.J. and Wilcox R.S. 2022 Phys. Plasmas 29 022507
- [49] Sweeney R. et al 2021 Nucl. Fusion 61 066040

IAEA-CN-316/2876

- $[50] \ \ Jepson \ J.R., Hegna \ C.C., Held \ E.D., Spencer \ J.A. \ and \ Lyons \ B.C. \ 2021 \ Phys. \ Plasmas \ 28 \ 082503$
- [51] Zhuang G. et al (the CFETR Design Team) 2019 Nucl. Fusion 59 112010
- [52] Glasser A.H., Greene J.M. and Johnson J.L. 1975 Phys. Fluids 18 875–88
- [53] Wesson J. 2011 Tokamaks 4th edn (Oxford University Press) ch. 4.4 and 4.9